Biophysical Journal
Article

Biophysical Society

Simultaneous assessment of membrane bilayer structure and drug insertion by ^{19}F solid-state NMR

Kiran Kumar,[1] Alexandre A. Arnold,[1] Raphaël Gauthier,[2] Marius Mamone,[2] Jean-François Paquin,[2] Dror E. Warschawski,[1,3,*] and Isabelle Marcotte[1,*]

[1]Departement of Chemistry, Université du Québec à Montréal, Montreal, Québec, Canada; [2]PROTEO, CCVC, Département de Chimie, Université Laval, Québec, Québec, Canada; and [3]Chimie Physique et Chimie du Vivant, CPCV, CNRS UMR 8228, Sorbonne Université, Ecole normale supérieure, PSL University, F-75005, Paris, France

ABSTRACT Fluorine-19 is an ideal nucleus for studying biological systems using NMR due to its rarity in biological environments and its favorable magnetic properties. In this work, we used a mixture of monofluorinated palmitic acids (PAs) as tracers to investigate the molecular interaction of the fluorinated drug rosuvastatin in model lipid membranes. More specifically, PAs labeled at the fourth and eighth carbon positions of their acyl chains were coincorporated in phospholipid bilayers to probe different depths of the hydrophobic core. First, the ^{19}F chemical shift anisotropy (CSA), indicative of membrane fluidity, was simultaneously determined for fatty acids (FAs) and the fluorinated drug using either slow magic-angle spinning (MAS) 1D ^{19}F solid-state NMR (SS-NMR) or MAS 2D ^{19}F-^{19}F SS-NMR with CSA recoupling. Membrane heterogeneity and selective partitioning of rosuvastatin into fluid regions could thus be evidenced. We then examined the possibility of mapping intermolecular distances in bilayers, in both the fluid and gel phases, using ^{19}F-^{19}F and ^{1}H-^{19}F correlation experiments by SS-NMR using MAS. Spatial correlations were evidenced between the two PAs in the gel phase, while contacts between the statin and the lipids were detected in the fluid phase. This work paves the way to mapping membrane-active molecules in intact membranes, and stresses the need for new labeling strategies for this purpose.

SIGNIFICANCE Lipid membranes ensure cell integrity and protection from their environment. They can be targeted or crossed by bioactive molecules, such as drugs, on their way to the target site. In this work, we exploit the high sensitivity of fluorine-19 and its low abundance in biological systems to study the membrane state and interactions with the fluorinated drug rosuvastatin at the nanoscopic level using ^{19}F solid-state NMR. We demonstrate that incorporating monofluorinated fatty acids at different positions on their acyl chains into lipid bilayers allows determining membrane fluidity. Moreover, we show that membrane-active molecules can be mapped within the bilayer through intermolecular ^{19}F-^{19}F and ^{19}F-^{1}H contacts. This approach could be applied to study intact cells.

INTRODUCTION

Solid-state NMR (SS-NMR) experiments can provide information on both structural and dynamical aspects of molecular interactions with biological membranes (1–5). In the case of complex cellular systems with many different constituents, determining the location of a guest molecule in the membrane is challenging. Notably, establishing the structural connectivity or distance relationships to the molecules found in the membranes, such as lipids, proteins, and carbohydrates, is particularly daunting. Depending on the experimental needs, different membrane mimetic systems can be employed (6). Rapidly reorienting model membranes such as a micelles, are readily accessible and amenable to ^{1}H-based solution NMR experiments, which allow fast signal acquisition and high spectral resolution (7,8). These experiments can be complemented by isotopic labeling strategies to constrain the structure of molecules or elucidate their spatial organization (7). However, such model systems reproduce the membrane poorly. Moreover, the NMR strategies that they enable cannot be applied to slow-tumbling lipid bilayers, such as multilamellar vesicles, and to whole cell membranes. Obtaining dynamical constraints and accurate distance measurements is difficult in such systems,

Submitted September 13, 2024, and accepted for publication November 26, 2024.

*Correspondence: dror.warschawski@sorbonne-universite.fr or marcotte.isabelle@uqam.ca

Editor: Leonid Brown.

https://doi.org/10.1016/j.bpj.2024.11.3319

particularly in the natural fluid state of the membrane where often both solution and SS-NMR experiments break down. From an NMR point of view, the challenges faced arise not only from low sensitivity and spectral overlap but also from motional and spatial heterogeneity.

In this regard, fluorine-19 (^{19}F) labeling of membrane lipids provides several benefits, notably its high sensitivity and absence in biological systems, thus limiting the possibility of signal overlap (9,10). The usefulness of fluorinated lipids and palmitic acid (PA) was demonstrated in our previous studies (11–15), notably the possibility to incorporate fluorine labels at different locations across red blood cell ghost membranes with a single monofluorinated PA probe on either carbons 4, 8, or 14 of the acyl chains (11). This allowed probing the interaction of an antimicrobial peptide at different locations of the membrane's hydrophobic core.

In this work, we extend our previous study by showing that the information offered by different ^{19}F-PAs can be simultaneously obtained in a multiply labeled model membrane. Furthermore, similar information can be obtained for the monofluorinated drug molecule rosuvastatin (RVS) inserted in the fluorinated membrane. This drug was selected because statins are well known for their pleiotropic action (16), which involves interaction with the lipid bilayer where they are known to modulate the structure and dynamics of membranes by exerting their effect on lipids or cholesterol (17,18) and even induce phase separation or the formation of lipid rafts in the membrane (16,17).

We then evaluate to what extent ^{19}F-^{19}F distances can be measured in a membrane environment in both the motionally restricted gel phase and the more native fluid phase. We exemplify these distance measurements by examining the proximity between ^{19}F-PAs and the monofluorinated RVS, which has been shown to insert in POPC (1-palmitoyl-2-oleoyl-glycero-3-phosphocholine) bilayers (17). Experiments are carried out under slow magic-angle spinning (MAS) conditions, which enable the measurement of anisotropic interactions with site-specific resolution of the various ^{19}F-PAs and statins. At faster although moderate spinning frequencies (∼10 kHz), only the central isotropic peak remains, and two-dimensional (2D) correlation experiments can be used either to measure recoupled chemical shift anisotropy (CSA) values with site-specific resolution or to elucidate molecular proximity.

Overall, we show that ^{19}F MAS SS-NMR of multiply labeled membranes can provide valuable information on molecular structure and proximity in an anisotropic lipid system, even in the fluid state. Accurate distance measurements are indeed possible in membranes by employing ^{19}F. However, additional hurdles such as unfavorable dynamics or phase separation need to be taken into account, especially in the case of whole-cell systems.

MATERIALS AND METHODS

Materials

All lipids and detergent molecules used in this study were obtained from Avanti Polar Lipids (Alabaster, AL), which include POPC and dodecylphosphocholine. RVS, sparfloxacin (SPX), deuterium-depleted water, as well as all other solvents and chemicals were purchased from Sigma-Aldrich (Oakville, ON, Canada). Deionized 18.2 MΩ cm Milli-Q water was used in all experiments (Millipore-Sigma). Monofluorinated fatty acids (FAs) were synthesized following a protocol detailed in Kumar et al. (11).

Multilamellar vesicles preparation

Multilamellar vesicles were prepared using the dry film method described by Warschawski et al. (19). In brief, the lipid mixture (including ^{19}F-labeled PAs) was dissolved in a 1:2 methanol/$CHCl_3$ solution and dried under nitrogen stream. Remaining traces of organic solvent in the lipid film were removed by high vacuum for at least 2 h. RVS or SPX dissolved in 1:2 methanol/$CHCl_3$ were directly added to the dry lipid film at a lipid/PAs/drug molar ratio of 40:20:3, followed by a 1–2-h solvent evaporation step. The mixed lipid film containing the drug was then hydrated with a physiologically relevant solution of 150 mM NaCl prepared with ^{2}H-depleted water if necessary. The lipid dispersion was submitted to a series of 3–5 cycles of freeze (10 min at −20°C), thaw (10 min above 40–55°C) and vortex shaking, and finally transferred into a 4-mm diameter (105 μL volume, 15 kHz maximum spinning frequency) or 1.9-mm diameter (15 μL volume, 42 kHz maximum spinning frequency) SS-NMR rotor.

SS-NMR experiments

All SS-NMR spectra were recorded using a Bruker Avance III-HD wide-bore 400 MHz spectrometer (Milton, ON, Canada) equipped with either a double-tuned 4-mm-HFX probe or a ^{1}H-^{19}F filter, allowing to observe ^{19}F with ^{1}H decoupling, or alternatively a 1.9-mm HXY probe converted into FXY probe, with no ^{1}H decoupling.

1D ^{19}F SS-NMR experiments were carried out at different MAS frequencies with a phase-cycled Hahn echo sequence. Static or 1 kHz ^{19}F spectra were collected with the 4-mm HFX probe using 1024 scans per spectrum, for a total acquisition time of 50 min with a recycle delay of 3 s. Static ^{19}F SS-NMR spectra were obtained using a phase-cycled Hahn echo pulse sequence, with an interpulse delay of 35 μs and high-power (50 kHz) ^{1}H decoupling during acquisition. The 90° pulse length was 4 μs and data were collected using 2048 points for ^{19}F SS-NMR with a recycle delay of 3 s. The ^{19}F chemical shifts were referenced to the trifluoroacetic acid signal at −76.5 ppm. The same probe was used to record 10 kHz MAS spectra, obtained with 128 scans and a total acquisition time of 6 min with a recycle delay of 3 s. For all ^{19}F MAS spectra, a minimum of 3k data points were collected, with a 4-μs 90° pulse length, and interpulse delays were rotor-synchronized. When necessary, ^{1}H-^{19}F cross-polarization (CP) was performed for 1 ms. Fast MAS at 33 kHz was carried out with a 1.9-mm FXY probe, and 1D ^{19}F spectra were collected using 32 scans and a total acquisition time of 2 min, without ^{1}H decoupling.

2D ^{19}F-^{19}F CSA recoupling sequence under MAS (FROCSA) was used with an 11 kHz MAS frequency on the 4-mm probe and ^{1}H decoupling without CP, analogous to the ^{31}P recoupling of chemical shift anisotropy sequence proposed by Warschawski et al. (19). Spectra were acquired with 16 scans for each of the 32 rows, and a recycle delay of 2 s, for a total time of 17 min. Processing was performed with automatic baseline correction and no line broadening.

2D ^{1}H-^{1}H nuclear Overhauser enhancement spectroscopy (NOESY) experiments were done at different mixing times at 10 kHz MAS frequency on the HFX probe, with a total of 1k data points × 512 increments, each with 16 scans, for a maximum acquisition time of 6.5 h. 2D ^{1}H-^{19}F heteronuclear

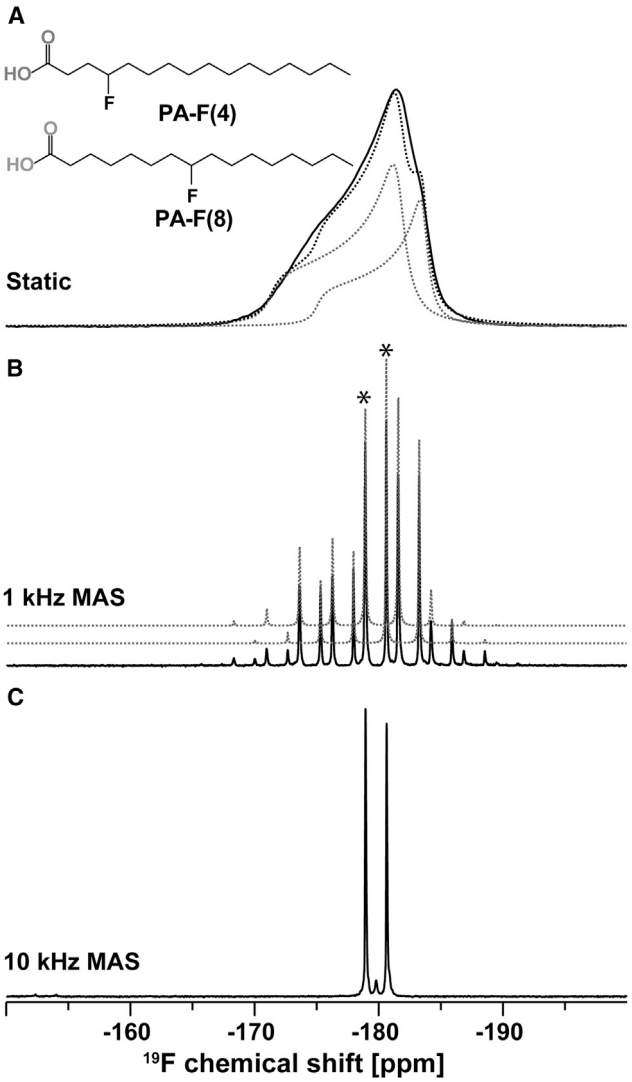

FIGURE 1 (*A*) Static, (*B*) 1 kHz, and (*C*) 10 kHz MAS ^{19}F SS-NMR spectra of POPC model membranes incorporating monofluorinated PAs, at a POPC/PA-F(4)/PA-F(8) molar ratio of 4:1:1. Experiments (*solid lines*) were performed at 35°C with ^{1}H decoupling. CSA values extracted from simulations (*dotted lines*) are indicated in Table 1.

Overhauser enhancement spectroscopy (HOESY) experiments were carried out with different mixing times and ^{1}H decoupling at 10 kHz MAS frequency on the HFX probe, with a total of 2k data points × 512 increments, each with 32 scans, for a maximum acquisition time of ∼35 h. For both experiments, a recycle delay of 2–3 s was used. 2D ^{19}F-^{19}F PDSD (proton-driven spin diffusion) with no recoupling at different MAS frequency on the HFX probe or with no ^{1}H decoupling at 33 kHz MAS frequency on the FXY probe. DARR (dipolar-assisted rotary resonance) with ^{1}H recoupling at different MAS frequency on the HFX probe, were carried out at various mixing times, with a total of 2k data points × 384 increments of 8 scans each, leading to a maximum of 2.5 h acquisition time, with a recycle delay of 2 s. When necessary, ^{1}H-^{19}F CP was performed for 1 ms. 2D ^{19}F-^{19}F RFDR experiments were done at 10 kHz MAS frequency on the HFX probe with 1k data points × 512 increments of 16 scans each, amounting to a maximum of 4.5 h of acquisition time, with 1 ms ^{1}H-^{19}F CP and a recycle delay of 3 s. For all experiments, the 50 kHz ^{1}H and 62.5 kHz ^{19}F RF field strengths were used and calibrated independently. Diagrams of all these pulse sequences are given in Fig. S1.

^{19}F CSA values were determined by line fitting using the Bruker Sola (Solid Lineshape Analysis) software. ^{1}H-^{1}H NOESY and ^{19}F-^{19}F PDSD or DARR buildup curves were generated using crosspeak volumes—after normalization by their diagonal peak volume and specific number of protons. Since there is no diagonal in the HOESY spectra, peak volumes were normalized by the most intense signal, which can be unambiguously assigned to aromatic protons of RVS (peaks n and o in Fig. S2).

Density functional theory

Geometry optimization of RVS or SPX were carried out by density functional theory (DFT) computations using the Gaussian 09 software suite (Carnegie Mellon University), B3LYP exchange correlation function, together with 6-311G basis set and default methanol or water as the solvation medium. By using these optimized minimum energy structures, magnetic shielding tensors were calculated by the GIAO B3LYP/CC-PVDZ method. Distances and isotropic shielding tensors obtained from DFT structural coordinates for both the investigated molecules were compared with the NMR results.

RESULTS AND DISCUSSION

Molecular dynamics through ^{19}F CSA measurement

Information at different depths of the lipid bilayer, previously recorded sequentially, were *simultaneously* obtained by incorporating PAs fluorinated at different positions in a phospholipid bilayer. Fig. 1 *A* shows the static ^{19}F SS-NMR spectra recorded as a function of temperature, of a POPC model membrane in which two types of PAs, fluorinated at position 4 or 8, are coincorporated. Two broad powder patterns are overlapped, but clearly shifted from one another and both can be deconvoluted through spectral fitting. Similarly to the values reported by Kumar et al. (11), a higher CSA value of ≈15–17 ppm was measured in the gel phase at −15°C and up to −3°C (Table 1). The CSA value dropped to 5–7 ppm in the fluid phase.

Two resonances were resolved using MAS (Fig. 1, *B* and *C*) and assigned to the two PAs, respectively fluorinated on positions 4 (δ_{iso} = −180.6 ppm) and 8 (δ_{iso} = –178.9 ppm), in agreement with our previous report (11). The site-specific CSA values can be determined by fitting the spinning sideband manifolds obtained at a low spinning frequency. As seen Fig. S3 and reported in Table 1, the spectra in the gel phase (−15 and −3°C) reveal a CSA value of ∼16 ppm for both PA-F(8) and PA-F(4). Note that the powder patterns of the two PAs cannot be resolved in the gel phase without MAS. In the fluid phase, the CSA values of both PAs are very close (6.3 and 6.8 ppm for PA-F(4) and PA-F(8), respectively) as expected for a fully miscible system and consistent with the pseudo-binary phase diagram of lipid membranes containing PAs (11,20). The remaining differences between the two CSAs can be ascribed to the differing fluorine position along the acyl chain. No superposition of gel and fluid phases was detected (11). The phase-transition temperature of POPC membranes without PAs is −2°C (21) and a temperature range of −15 to 35°C appears to be

TABLE 1 ^{19}F CSA values (in ppm, with standard deviation) of monofluorinated PAs and RVS in model membranes, with or without RVS, at various temperatures, measured by three different methods

		Static			Slow MAS			FROCSA		
Temperature (°C)	Sample	PA-4	PA-8	RVS	PA-4	PA-8	RVS	PA-4	PA-8	RVS
35	without	5.4 (0.5)	7.2 (0.5)	–	6.3 (0.3)	6.8 (0.9)	–	6.7 (0.6)	7.1 (0.7)	–
	with RVS	4.9 (0.1)	4.3 (0.3)	7.5 (0.1)	5.8 (0.8)	5.6 (1.4)	7.4 (0.8)	6.1 (0.9)	5.9 (0.4)	6.9 (1.5)
−3	without	16.7 (0.2)		–	16.7 (1.0)	16.5 (0.7)	–	16.7 (0.2)	17.1 (0.8)	–
	with RVS	15.1 (0.4)		8.2 (0.3)	15.4 (0.6)	16.9 (0.1)	7.7 (0.4)	15.3 (0.4)	17.0 (0.1)	7.3 (0.3)
−15	without	16.6 (0.8)		–	17.3 (0.3)	16.8 (1.1)	–	16.9 (0.5)	17.2 (0.6)	–
	with RVS	16.3 (0.2)		–	16.1 (0.1)	17.0 (0.1)	–	15.5 (0.5)	17.4 (0.6)	–

appropriate for studying the phase behavior of PA-containing lipid membrane by ^{19}F static spectra.

In the case of slow-MAS spectra, CSA values closely agree with those obtained from the static spectra through spectral fitting. Since the CSA is almost completely averaged-out at a spinning frequency of 10 kHz (Fig. 1 *C*), the best MAS frequency to be used for a CSA analysis is a compromise between sensitivity (higher intensity for a reduced number of spinning sidebands) and precision in the CSA measurement (increased number of sidebands). In a model membrane with a high ^{19}F-PA proportion (33 mol %), spinning frequencies on the order of 1–2 kHz are adequate, but higher MAS frequencies are likely to be necessary in whole cells.

Alternatively, 2D experiments that can recouple the CSAs under fast MAS and separate them according to their isotropic chemical shift have been developed for ^{13}C and ^{31}P SS-NMR (19,22). This ROCSA experiment is adapted here to ^{19}F SS-NMR (Fig. 2), which we coin "FROCSA" for simplicity. As shown in Fig. 2, the CSAs of both fluorinated PAs can be obtained in less than 20 min, at a spinning frequency of 11 kHz. We would like to stress that since 2D FROCSA can provide CSA values at higher MAS frequencies, the total experimental time is reduced compared with the 1D slow MAS experiments. As shown in Table 1, the CSAs extracted from the slow-spinning or the FROCSA experiments are in excellent agreement. When a single FA species is present, the CSAs extracted from the static spectra are also in good agreement. However, as might be expected, the discrepancy increases when the two FAs signals overlap in static spectra and in this case, CSA obtained through slow spinning or FROCSA are more reliable. The site-specific information obtainable through slow spinning or FROCSA should also be accessible with other membrane mimetics or whole cell samples.

The ^{19}F nucleus on phospholipid or FA acyl chains is particularly sensitive to the bilayer ordering, as we previously demonstrated with red blood cell ghosts (11). It is also interesting to monitor the influence of a fluorinated molecule on the phase transition of the membrane in which it is incorporated. Indeed, a great number of membrane-active drugs are fluorinated (17,23,24) and their ^{19}F NMR spectra have been shown to help assess their membrane interaction (23,24). Due to the strong structure dependence of ^{19}F isotropic chemical shifts, values for drugs are likely to differ from those of ^{19}F-labeled acyl chains in lipids or FAs. It should therefore be possible to simultaneously investigate the structure and dynamical properties of both a membrane-active drug and the hydrophobic core of the membrane—as revealed by ^{19}F-labeled acyl chains—using the same ^{19}F SS-NMR spectrum.

We thus examined the monofluorinated RVS, incorporated in POPC/^{19}F-PA model membranes. As shown in Fig. 3, the ^{19}F signals of RVS as well as PA-F(4)'s and PA-F(8)'s are well separated and, using slow MAS, the CSA values of all fluorinated species could be measured (Table 1). The FROCSA experiment could also be used for this system, as shown in Fig. 4. Our results indicate that the ^{19}F CSA values of the FAs below and above the main melting temperature of the membrane are minimally reduced in the presence of the statin (∼0.5 to 1 ppm). Interestingly, the CSA of the statin, which is axially symmetric and similar in width to the one of the FAs above the T_m, is only slightly modified when the temperature is reduced to −3°C. The asymmetry is small (∼0.2), and the CSA value increases only by 1 ppm, whereas the FAs' CSA values are multiplied by almost a factor of 3. The statin, thus, appears to remain mostly in a fluid environment, most likely segregated from PA-rich gel phase regions of the membrane. At an even lower temperature (−15°C), the CSA of RVS increases drastically, and its signal becomes barely detectable under static conditions, or disappears under slow MAS (Fig. S3). The most probable explanation for the latter observation is that short transverse relaxation prevents MAS averaging. It should be stressed that site-specific CSA values at lower temperatures are accessible either with slow MAS or FROCSA experiments (Figs. 3 and 4). In the case of whole-cell membrane studies, where sensitivity is a key issue, 2D FROCSA will be preferred because it can provide CSA values faster than with 1D slow MAS experiments.

Using a model membrane with multiple ^{19}F labels, a simple slow MAS ^{19}F spectrum or FROCSA can thus be used to assess the local dynamics of the bilayer's hydrophobic core, and thereby evaluate membrane heterogeneity and drug location simultaneously. Further insights might be obtained by determining ^{19}F-^{19}F internuclear distances.

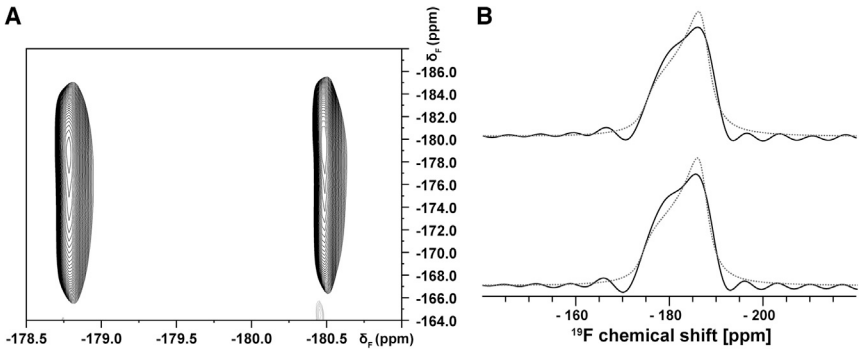

FIGURE 2 (*A*) 2D ^{19}F-^{19}F FROCSA spectrum and (*B*) 1D ^{19}F slices extracted from the 2D NMR spectrum of POPC model membranes incorporating monofluorinated PAs, at a POPC/PA-F(4)/PA-F(8) molar ratio of 4:1:1. Experiments (*solid lines*) were performed at 11 kHz MAS with ^{1}H decoupling, at 35°C. CSA values extracted from simulations (*dotted lines*) are indicated in Table 1.

Membrane molecular structure through ^{19}F-^{19}F distance measurements

A more accurate description of the membrane structuring might be obtained by assessing ^{19}F-^{19}F internuclear distances (or, semiquantitatively, proximities) between FAs and between the FAs and a membrane-active drug. The accurate measurement of such distances in membrane samples is, however, notoriously difficult, in particular due to the dynamics in hydrated fluid biomembranes. The ideal type of experiment to use needs to be determined and, most importantly, a single set of experiments might not be valid in both the gel and the fluid phases.

In SS-NMR, distances are usually obtained through magnetization transfer, the mechanism of which depends on the physical state of the sample, and two situations can be distinguished. In the case of rigid molecules, distances can be deduced from the measurement of coherent dipolar couplings between isolated spins, through dipolar recoupling sequences such as R2 (rotational resonance), REDOR (rotational-echo double resonance), or RFDR (radiofrequency-driven recoupling), for example. Some 2D SS-NMR sequences also allow the detection of correlations between spins that are not directly coupled, using spin diffusion. The most frequently used sequences of this type are ^{13}C-^{13}C PDSD (proton-driven spin diffusion) and DARR. On the contrary, in the presence of molecular motion, coherent dipolar couplings are averaged out, and distances can be obtained by measuring dipolar couplings indirectly through NOE effects and, to some extent, spin diffusion. Diagrams of all these pulse sequences are given in Fig. S1. Membranes in the gel phase belong to the category where R2, REDOR, RFDR, DARR, or PDSD have been used to measure distances in lipids (25–27) and peptides (25,28–35). In the fluid phase, ^{1}H-^{1}H NOESY under MAS has been employed to study lipid structure and dynamics, and the relative effects of NOE and spin diffusion (36–38). Ramamoorthy and Xu also used this approach for the structural assessment of a membrane-bound antimicrobial peptide (39).

Here, we examined the possibility of measuring intermolecular distances between monofluorinated FAs, or between a fluorinated drug and an FA, to determine the membrane structure or drug location. All our attempts to detect ^{19}F-^{19}F correlations (using RFDR, PDSD, or DARR) between FAs in the model POPC/FA membranes in the fluid state have failed (data not shown). We therefore considered membranes in the gel state, at −3°C as generally done in the literature to determine intermolecular distances (26). It was not possible to establish spatial correlations between FAs through direct ^{19}F-^{19}F dipolar couplings via RFDR (data not shown). However, 2D ^{19}F-^{19}F PDSD and DARR correlation spectra of fluorinated PAs incorporated in POPC membranes could be obtained. In the gel state, peaks are well resolved, and correlations between ^{19}F nuclei at positions 4 and 8 are clearly visible. However, DARR crosspeaks, when ^{1}H recoupling is performed, are weaker than those observed on the PDSD spectrum (compare Fig. 5, *A* and *C*).

To estimate the distance between fluorinated FAs in lipid membranes, we used the crosspeaks' buildup rates since they are related to internuclear distances. To do so, we first calibrated the ^{19}F-^{19}F buildup rates in a standard molecule containing a fixed and known ^{19}F-^{19}F distance. For this purpose, we selected the bifluorinated antibiotic SPX, with an internuclear distance of 4.73 Å (Fig. S5) determined by DFT and measured by RFDR (Fig. S6). Although the two systems must be compared with caution, one can assume that the slower PDSD magnetization transfer between PA-F(4) and PA-F(8) shown in Fig. 5 *B* is indicative of a longer average intermolecular distance as compared with the intramolecular distance between the two fluorines of SPX in a (2:1) dipalmitoylphosphatidylcholine/SPX mixture, observed in Fig. S6, i.e., longer than 4.7 Å.

In no case under our experimental conditions was a correlation between the drug and any of the FAs observed. Overall, the fact that a PA-F(4)/PA-F(8) distance can be measured, while no proximity between either PAs and the statin is observed, likely results from a phase separation between PAs partitioning into the gel phase, and statin partitioning into the fluid phase. While this information could already be inferred from the lineshape analysis of the 1D spectra, these results are a clear indication that a ^{19}F-^{19}F distance with a labeled PA can be measured within the bilayer.

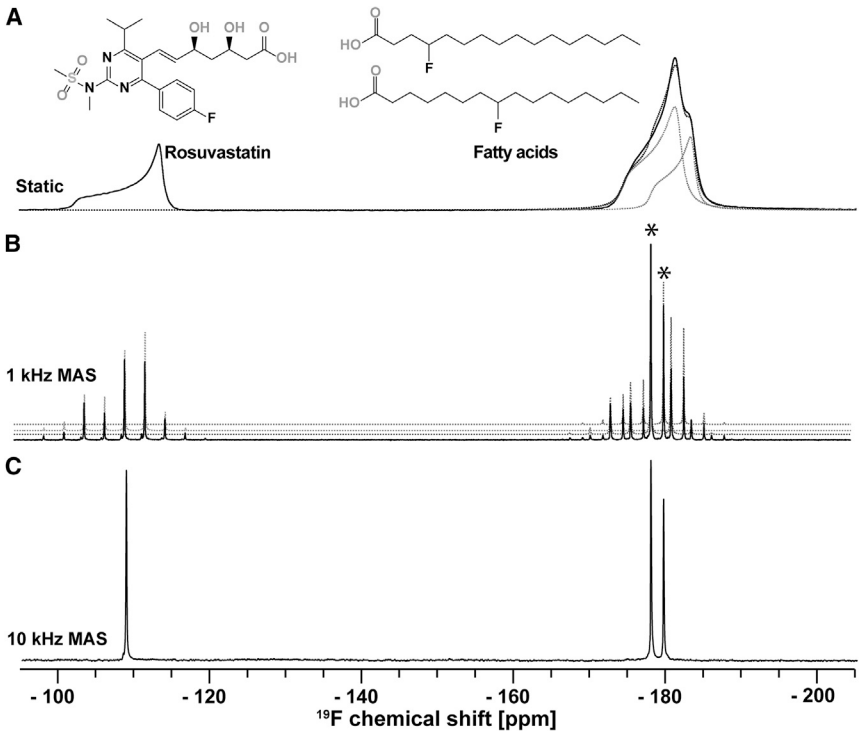

FIGURE 3 (*A*) Static, (*B*) 1 kHz, and (*C*) 10 kHz MAS ^{19}F SS-NMR spectra of POPC model membranes incorporating monofluorinated PAs, at a POPC/PA-F(4)/PA-F(8) molar ratio of 4:1:1, with rosuvastatin at a lipid/PAs/RVS molar ratio of 40:20:3. Experiments (*solid lines*) were performed with ^{1}H decoupling at 35°C. CSA values extracted from simulations (*dotted lines*) are indicated in Table 1. PA resonances are on the right (approximately −180 ppm), while statin resonances are on the left (approximately −105 ppm).

Admittedly, this type of information will become valuable if a distance can be measured between an FA and a guest molecule in the same membrane phase.

These results raise the question of the magnetization transfer mechanism between fluorine spins. Lipid membranes form 2D liquid crystals with various types of motions depending on the phase. At −3°C, the POPC/PA membrane exhibits motional restriction characteristic of the gel phase (Table 1), at least in the PA-rich regions. Interestingly, ^{19}F PA(4)-PA(8) crosspeaks could only be detected in the gel phase. The fact that only this solid-like state provides the appropriate dynamical regime for magnetization transfer to occur is a good indication that ^{19}F-^{19}F NOE or ^{1}H spin diffusion are not efficient transfer mechanisms at higher temperatures. Moreover, the intermolecular distance in this case is likely beyond the longest distance detectable by ^{19}F-^{19}F NOE, which can be estimated to 4–5 Å. In addition to dynamical considerations, Roos et al. (40) have shown that two scenarios need to be considered when measuring ^{19}F-^{19}F internuclear distances: one in which the isotropic chemical shifts are identical, and one where they significantly differ. In the first case, magnetization transfer without ^{1}H-^{1}H recoupling (PDSD) is optimal and is thus CSA-mediated while, in the second case, ^{1}H-^{1}H recoupling (DARR) accelerates this transfer, which is therefore mediated by dipolar couplings. The effect of ^{1}H-^{1}H recoupling is thus a good criterion to determine the regime in which a given ^{19}F pair is.

In the gel phase, without ^{1}H recoupling, the buildup of the off-diagonal ^{19}F-^{19}F PDSD crosspeak intensities reaches a plateau at a mixing time of 200–300 ms, with a maximum transfer of 50% at 10 kHz MAS frequencies, and of 80% at a slower 3.3 kHz MAS (Fig. 5 *B*). The reintroduction of ^{1}H-^{1}H dipolar couplings in DARR clearly reduces the magnetization transfer, as the maximum transfer at 200 ms reaches 20% at 10 kHz, and 75% at slower 3.3 kHz MAS (Fig. 5 *D*). While in the case of ^{13}C SS-NMR, DARR has been shown to accelerate spin exchange (41), the behavior observed here is reminiscent of that observed for ^{19}F spins with the same isotropic chemical shift and different chemical shift anisotropies, where the absence of ^{1}H-^{1}H irradiation accelerates the buildup rate by up to a factor of 5 (40). The small difference in isotropic chemical shifts (1.7 ppm) between the PAs labeled on positions 4 and 8, thus appears to be sufficiently small to favor this type of CSA-mediated spin diffusion. For this situation, the ^{19}F CODEX experiment at high MAS frequencies should enable the detection of longer distances (40), a potentially interesting avenue which we could not test for lack of an appropriate probe. No crosspeak intensity between FAs and the statin could be detected with mixing times of up to 750 ms (data not shown). The strong discrepancy in isotropic chemical shifts (∼80 ppm) most likely prevents the same type of phenomenon to take place.

Localization of fluorinated molecules in a lipid bilayer

Our primary goal for ^{19}F labeling was to map the insertion of a guest molecule (drug or peptide) within the membrane

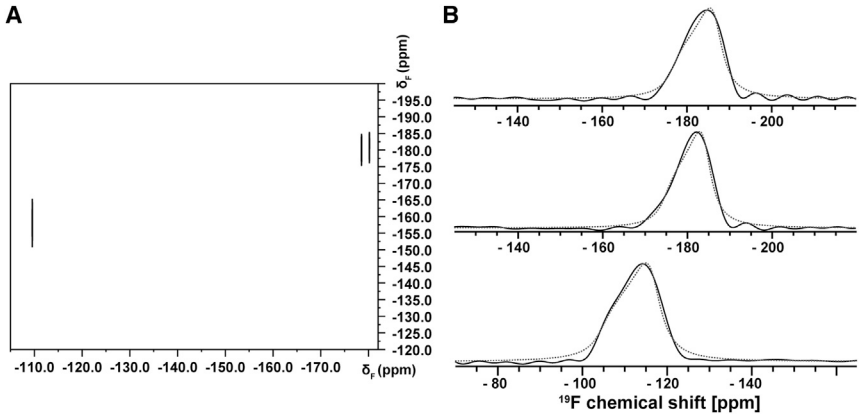

FIGURE 4 (*A*) 2D ^{19}F-^{19}F FROCSA spectrum and (*B*) 1D ^{19}F slices extracted from the 2D NMR spectrum of POPC model membranes incorporating monofluorinated PAs, at a POPC/PA-F(4)/PA-F(8) molar ratio of 4:1:1, with rosuvastatin at a lipid/PAs/RVS molar ratio of 40:20:3. Experiments (*solid lines*) were performed at 11 kHz MAS with ^{1}H decoupling at 35°C. CSA values extracted from simulations (*dotted lines*) are indicated in Table 1. PA resonances are on the right (approximately −180 ppm), while statin resonances are on the left (approximately −105 ppm).

by determining its distance relatively to ^{19}F atoms located at various positions on the FA acyl chain. As demonstrated in the previous section, it should indeed be possible using a POPC/^{19}F-PA system. We thus attempted to locate RVS in the bilayer, using ^{19}F SS-NMR. The phase separation into PA-rich gel phase regions and POPC-rich fluid ones—in which the statin preferably partitions—prevents the measurement of RVS-PA distances. By increasing the temperature, the bilayer can be made homogeneous but, unfortunately, in the fluid state, local motions drastically reduce coherent dipolar couplings and CSA, to the extent that standard SS-NMR techniques break down. Overhauser effect cross-relaxation, on the other hand, has been shown to be efficient in fluid membranes, and ^{1}H-^{1}H homonuclear NOESY has indeed been used to locate statin molecules in lipid bilayers (17).

Fig. S7 shows that ^{1}H-^{1}H NOEs could effectively be detected within the aromatic ring of RVS, as well as between RVS's aromatic protons and the lipids' protons, including the acyl chains. An NMR study by Galiullina et al. (17) also showed similar cross correlation effects between POPC and RVS, while the authors were using membranes without PAs. In our case, whether these acyl chains belong to POPC or to the FAs could not be determined at this stage due to spectral overlap. Likewise, it was not possible through ^{1}H-^{1}H NMR to establish spatial proximities between FAs. As might be expected, the intramolecular cross-peak buildup is fast within the aromatic ring of RVS, which

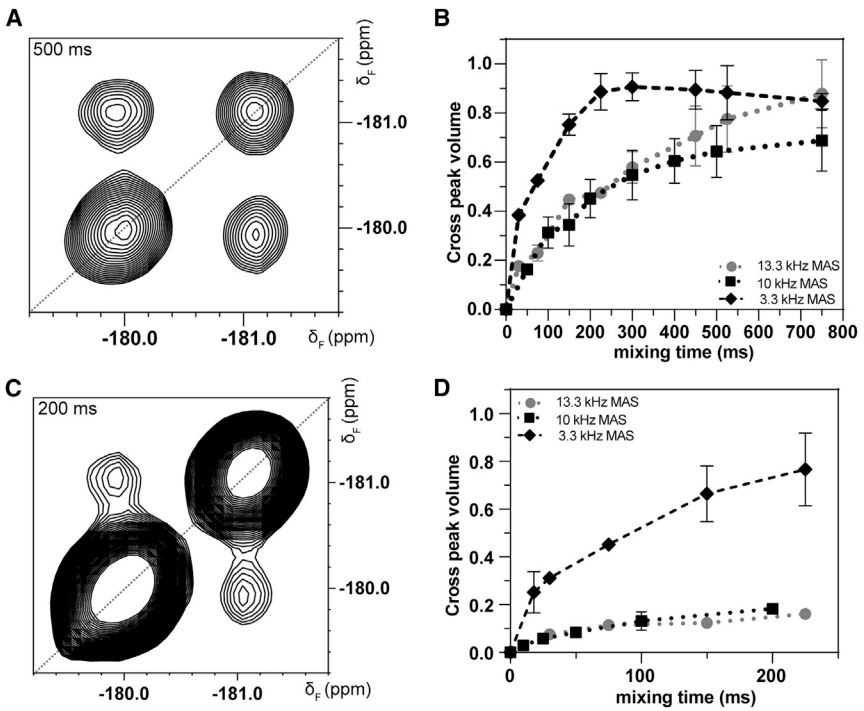

FIGURE 5 2D ^{19}F-^{19}F SS-NMR spectra of monofluorinated PAs incorporated in POPC membranes at a POPC/PA-F(4)/PA-F(8) molar ratio of 4:1:1. (*A*) PDSD at 500 ms mixing time and 10 kHz MAS and (*B*) PDSD buildup curves at different MAS rates. (*C*) DARR at 200 ms mixing time and 10 kHz MAS and (*D*) DARR buildup curves at different MAS rates. Experiments were performed at −3°C with ^{1}H decoupling during acquisition. Error bars represent standard deviation on the mean (n = 2).

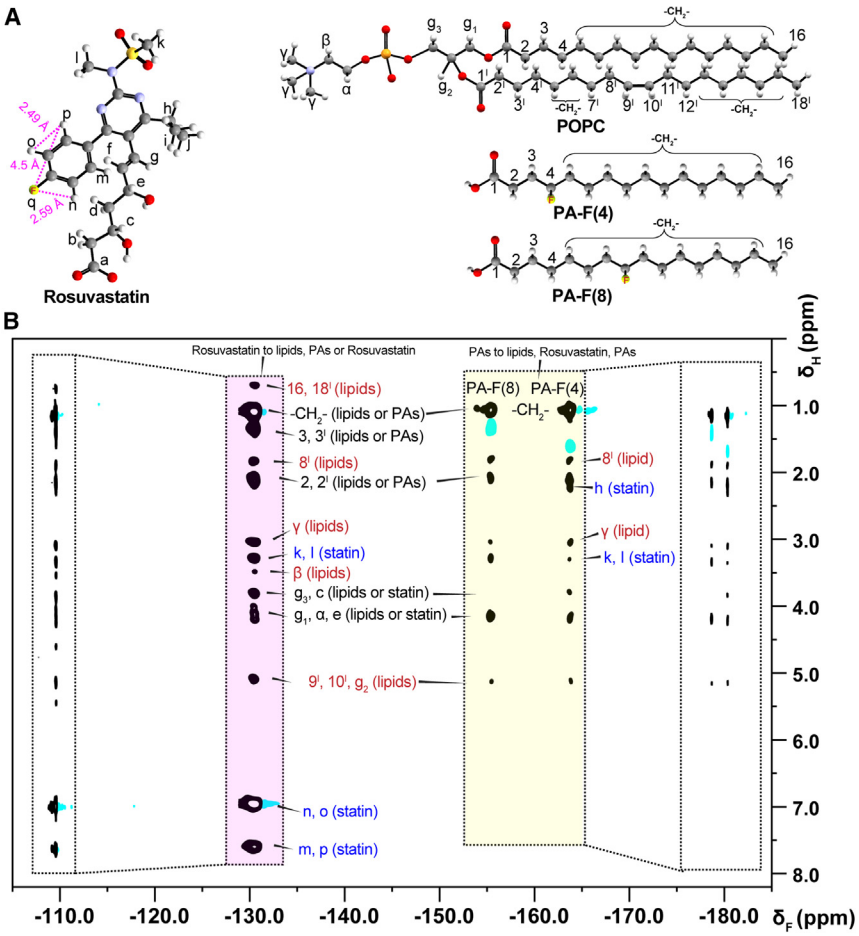

FIGURE 6 (*A*) DFT optimized structure of RVS and manually modeled structure of POPC and PAs with annotation. (*B*) 10 kHz MAS ^{1}H-^{19}F 2D HOESY spectrum, with 500 ms mixing time, of rosuvastatin incorporated into POPC/PA-F(4)/PA-F(8) at a 4:1:1 molar ratio, with a lipid/PAs/RVS molar ratio of 40:20:3. Experiments were performed at 35°C. Black peaks are positive crosspeaks. Blue peaks are negative signals that can be considered as artifacts.

reaches a plateau at a mixing time of ∼500 ms, corresponding to a distance of ∼2.49 Å. A much slower buildup was observed between these aromatic ^{1}H and those of the choline headgroup, the glycerol and the terminal acyl methyl group, with a slightly faster buildup for the statin to glycerol (g_2) NOE. An intermolecular distance between 2.5 and 5 Å is thus expected. The precise location of RVS with respect to the bilayer core cannot be determined, since contacts are evidenced with both the headgroup, middle section and acyl chains. One might also consider the presence of spin diffusion, which would prevent any such precise conclusions. Moreover, faster buildups of the crosspeaks between the statin-protons and 8^{l} acyl chain protons, and with the g_2 protons were noticeable and thus, statins are likely positioned closer to these two protons, in the upper part of the membrane.

The use of ^{19}F-labeled FAs also enables the measurement of ^{1}H-^{19}F distances using HOESY in the fluid phase—the natural state of biological membranes. The maximum distance that ^{1}H-^{19}F Overhauser effect allows to probe probably lies slightly below the 5 Å standard upper distance stated for the ^{1}H-^{1}H case. The main advantage of using ^{19}F NMR is the reduction in spectral overlap, easily enabling the identification of fluorinated molecules including FAs—a key feature if the measurements are performed in a complex environment such as native whole-cell membranes. 2D HOESY could be acquired starting with either ^{1}H or ^{19}F magnetization. We have tried the former for a stronger signal, but the latter could help alleviate ^{1}H-^{1}H spin diffusion.

Fig. 6 shows a ^{1}H-^{19}F 2D HOESY spectrum with a mixing time of 500 ms of RVS incorporated into POPC/PA-F(4)/PA-F(8) membranes, at 35°C and MAS at 10 kHz. Intermolecular contacts between the statin's ^{19}F atom at around −110 ppm and the ^{1}H of acyl chains are readily detectable and easy to identify. The buildup of characteristic statin intramolecular crosspeaks, as well as intermolecular statin crosspeaks with choline, glycerol and acyl chain terminal groups are shown in Fig. 7, *A* and *C*. The fastest buildups are, of course, the intramolecular ones, between the statin ^{19}F and aromatic protons, followed by the intermolecular crosspeak between the statin ^{19}F and the 8^{l} proton on the lipid acyl chain, again asserting statin location in the bilayer.

These ^{1}H-^{19}F results enable a more precise characterization of the statin insertion than by using the traditional

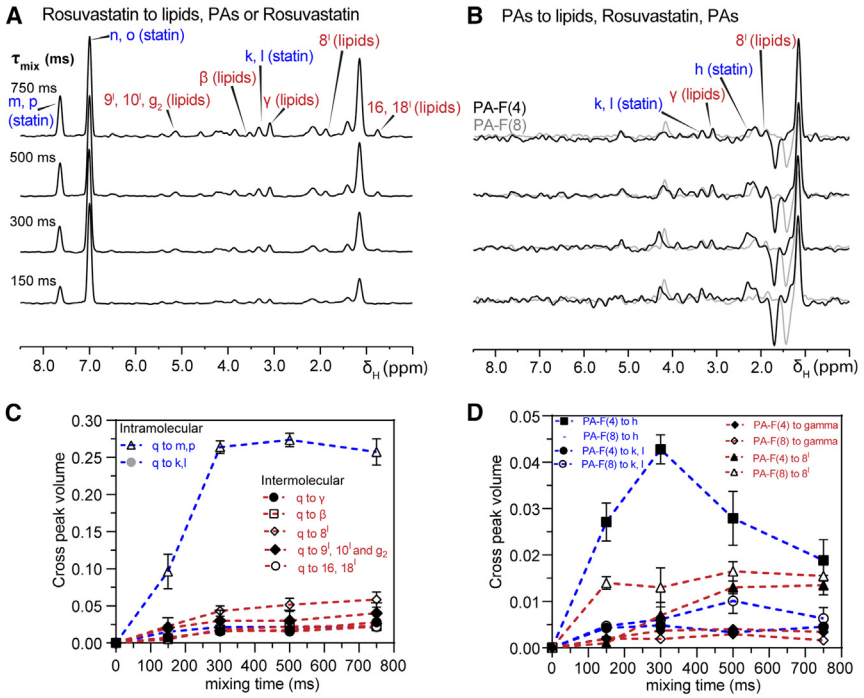

FIGURE 7 1D ^{1}H slices from the 10 kHz 2D ^{1}H-^{19}F HOESY at different mixing times, of rosuvastatin incorporated into POPC/PA-F(4)/PA-F(8) at 4:1:1, with a lipid/PAs/RVS molar ratio of 40:20:3 (*A*) at the ^{19}F chemical shift of statin, and (*B*) at the ^{19}F chemical shift of PAs. 10 kHz 2D ^{1}H-^{19}F HOESY buildup curves between (*C*) the fluorine of statin to aromatics protons of statins and lipid protons and (*D*) the fluorine of PAs to protons of statins and lipids. Peak integral is normalized to n, o peaks (∼2.59 Å). Error bars represent standard deviation on the mean (n = 2). All experiments were performed at 35°C with ^{1}H decoupling.

^{1}H-^{1}H approach. Indeed, the intermolecular buildup provides an estimate on the distance, which falls below the longest intramolecular distance of ∼4.5 Å and also sets an upper limit as to the distances that can be probed. Crosspeaks with a slow buildup are observed between methyl groups (k, l) of RVS and both PAs, indicating that RVS is located close to the fourth and eighth carbons of the acyl chains in the membrane. In addition, both ^{19}F atoms of PAs give strong correlations to 8^{l} protons of lipids, confirming their close proximity to POPC lipids and that they are no longer segregated in the fluid phase. A crosspeak with fast buildup is noticeable between the PA-F(4) to RVS's methylene (h), while no crosspeak is observed between (h) and PA-F(8), indicating the proximity of (h) and PA-F(4) (Fig. 7, *B* and *D*). Although, Galiullina et al. (17) locate RVS close to the C2-C3 segments of POPC, the presence of intramolecular cross-correlation such as h, d, and b (Figs. S2 and S7) limits the identification of a precise location of RVS by ^{1}H-^{1}H experiments. While direct ^{19}F-^{19}F experiments could not locate the drug in the fluid state, the depth of penetration of this statin into the bilayer can be established by ^{1}H-^{19}F experiments. A cartoon of its location is presented in Fig. 8. Alternatively, one could also consider paramagnetic probes to assess the insertion depth of a membrane-bound molecule (42,43). However, in the case of a charged molecule, we believe that ^{19}F labels reduce ambiguities that might arise from electrostatic interactions with the paramagnetic ions. In addition, fluorine probes, being more specifically localized within the membrane than ions, are likely to provide a more precise determination of the membrane-bound molecule's location.

CONCLUSION

This work showed that the incorporation in model membranes of FAs with ^{19}F labels at different positions on the acyl chain allows studying the interaction of host molecules. Structural questions were addressed by measuring ^{19}F-^{19}F distances, or at least enabled the establishment of spatial proximities. Below the phase transition temperature of POPC, phase separation was evidenced by detecting spatial contacts between PAs, but no contact between PAs and RVS. Magnetization transfer mechanisms were carefully analyzed in the fluid phase. We showed that one could only rely on NOEs, and demonstrated the advantages of using ^{1}H-^{19}F NOEs, easing spectral assignment and greatly reducing spectral overlap.

The use of ^{19}F labels could help in other similar cases, such as protein-ligand interactions in the membrane, or to locate molecules interacting with whole cells by SS-NMR. For the latter, it would require two strategies. First, to measure internuclear distances in conditions as native as possible, i.e., in the fluid phase. Heteronuclear ^{1}H-^{19}F NOEs could be used. This implies the development of more fluorination sites in the molecule of interest, to make distance measurements amenable. A second strategy would be to use SS-NMR approaches, by first freezing down membrane motions, while maintaining membrane structure and preventing phase separation or conformational changes. In addition, one might also use isotopic enrichment such as ^{13}C and ^{15}N, along with multiple fluorinations (44), which enables the measurement of internuclear distances using dipolar or scalar-based 2D or 3D experiments (44,45).

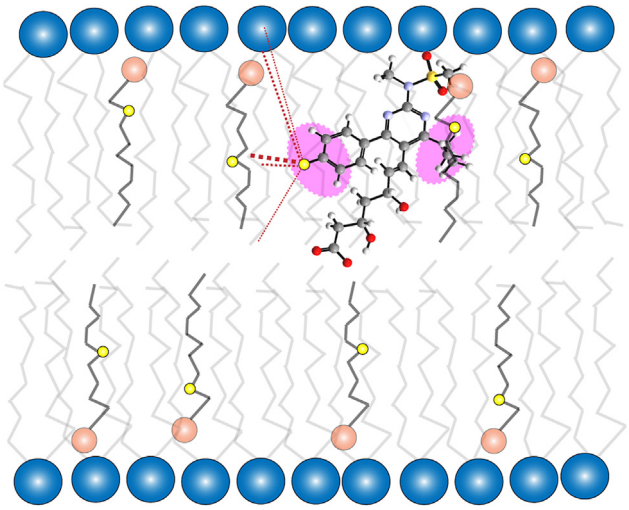

FIGURE 8 Schematic representation of RVS the in lipid bilayer. Shaded regions represent close proximity between nuclei as derived from ^{1}H-^{19}F NOE peaks. PC headgroups are represented by blue spheres, carboxylic acid headgroups in orange, and fluorine atoms in yellow. To provide a qualitative sense of drug's depth within the membrane, the thickness of the red dotted lines showing the internuclear contacts corresponds to the ^{1}H-^{19}F NOE's intensity.

ACKNOWLEDGMENTS

This research was funded by the Natural Sciences and Engineering Research Council (NSERC) of Canada (grant RGPIN-2018–06200 to I.M.) and the Centre National de la Recherche Scientifique (UMR 7203 to D.E.W.). K.K. would like to thank the Quebec Network for Research on Protein Function, Engineering, and Applications (PROTEO) —strategic cluster of the Fonds de recherche du Québec –Nature et technologies (FRQNT) —for the award of a scholarship. The authors thank Pierre Audet and Université Laval for the loan of the HFX probe.

AUTHOR CONTRIBUTIONS

K.K., A.A.A., D.E.W., J.-F.P., and I.M. conceptualized the project and established the methodology. I.M. acquired funding and administrated the project. A.A.A., D.E.W., J.-F.P., and I.M. supervised the project. K.K., R.G., M.M., and A.A.A. performed the experiments. K.K. and A.A.A. validated and analyzed the data. K.K. wrote the first draft, and all authors reviewed and edited the final text.

DECLARATION OF INTERESTS

The authors declare no competing interests.

SUPPORTING MATERIAL

Supporting material can be found online at https://doi.org/10.1016/j.bpj.2024.11.3319.

REFERENCES

1. Porcelli, F., R. Verardi, …, G. Veglia. 2008. NMR structure of the cathelicidin-derived human antimicrobial peptide LL-37 in dodecylphosphocholine micelles. *Biochemistry.* 47:5565–5572.
2. Nielsen, N. C., A. Malmendal, and T. Vosegaard. 2004. Techniques and applications of NMR to membrane proteins. *Mol. Membr. Biol.* 21:129–141.
3. Aucoin, D., D. Camenares, …, S. O. Smith. 2009. High-resolution ^{1}H MAS RFDR NMR of biological membranes. *J. Magn. Reson.* 197:77–86.
4. Mandala, V. S., J. K. Williams, and M. Hong. 2018. Structure and dynamics of membrane proteins from solid-state NMR. *Annu. Rev. Biophys.* 47:201–222.
5. Molugu, T. R., S. Lee, and M. F. Brown. 2017. Concepts and methods of solid-state NMR spectroscopy applied to biomembranes. *Chem. Rev.* 117:12087–12132.
6. Warschawski, D. E., A. A. Arnold, I. Marcotte…, 2011. Choosing membrane mimetics for NMR structural studies of transmembrane proteins. *Biochim. Biophys. Acta Biomembr.* 1808:1957–1974.
7. Marassi, F. M., and S. J. Opella. 1998. NMR structural studies of membrane proteins. *Curr. Opin. Struct. Biol.* 8:640–648.
8. Warnet, X. L., A. A. Arnold, …, D. E. Warschawski. 2015. In-cell solid-state NMR: an emerging technique for the study of biological membranes. *Biophys. J.* 109:2461–2466.
9. Macdonald, P. M., B. D. Sykes, F. D. Gunstone…, 1985. ^{19}F NMR studies of lipid fatty acyl chain order and dynamics in *Acholeplasma laidlawii* B membranes. Orientational order in the presence of a series of positional isomers of cis-octadecenoic acid. *Biochemistry.* 24:177–184.
10. Gent, M. P., P. F. Cottam, and C. Ho. 1978. Fluorine-19 nuclear magnetic resonance studies of *Escherichia coli* membranes. *Proc. Natl. Acad. Sci. USA.* 75:630–634.
11. Kumar, K., A. A. Arnold, …, I. Marcotte. 2024. ^{19}F solid-state NMR approaches to probe antimicrobial peptide interactions with membranes in whole cells. *Biochim. Biophys. Acta Biomembr.* 1866:184269.
12. Gagnon, M.-C., E. Strandberg, …, M. Auger. 2018. New insights into the influence of monofluorination on dimyristoylphosphatidylcholine membrane properties: A solid-state NMR study. *Biochim. Biophys. Acta Biomembr.* 1860:654–663.
13. Gagnon, M.-C., P. Ouellet, …, J.-F. Paquin. 2018. Towards the use of monofluorinated dimyristoylphosphatidylcholines as ^{19}F NMR reporters in bacterial model membranes. *J. Fluor. Chem.* 206:43–47.
14. Gagnon, M.-C., B. Turgeon, …, J.-F. Paquin. 2014. Evaluation of the effect of fluorination on the property of monofluorinated dimyristoylphosphatidylcholines. *Org. Biomol. Chem.* 12:5126–5135.
15. Guimond-Tremblay, J., M.-C. Gagnon, …, J.-F. Paquin. 2012. Synthesis and properties of monofluorinated dimyristoylphosphatidylcholine derivatives: Potential fluorinated probes for the study of membrane topology. *Org. Biomol. Chem.* 10:1145–1148.
16. Penkauskas, T., A. Zentelyte, …, G. Preta. 2020. Pleiotropic effects of statins via interaction with the lipid bilayer: A combined approach. *Biochim. Biophys. Acta Biomembr.* 1862:183306.
17. Galiullina, L. F., H. A. Scheidt, …, V. Klochkov. 2019. Interaction of statins with phospholipid bilayers studied by solid-state NMR spectroscopy. *Biochim. Biophys. Acta Biomembr.* 1861:584–593.
18. Kuba, J. O., Y. Yu, and J. B. Klauda. 2021. Estimating localization of various statins within a POPC bilayer. *Chem. Phys. Lipids.* 236:105074.
19. Warschawski, D. E., A. A. Arnold, and I. Marcotte. 2018. A new method of assessing lipid mixtures by ^{31}P magic-angle spinning NMR. *Biophys. J.* 114:1368–1376.
20. Inoue, T., S. Yanagihara, …, M. Suzuki. 2001. Effect of fatty acids on phase behavior of hydrated dipalmitoylphosphatidylcholine bilayer: saturated versus unsaturated fatty acids. *Chem. Phys. Lipids.* 109:117–133.
21. Liu, H., G. D. Bachand, …, D. Y. Sasaki. 2008. Lipid nanotube formation from streptavidin− membrane binding. *Langmuir.* 24:3686–3689.
22. Chan, J. C. C., and R. Tycko. 2003. Recoupling of chemical shift anisotropies in solid-state NMR under high-speed magic-angle spinning and in uniformly ^{13}C-labeled systems. *J. Chem. Phys.* 118:8378–8389.

23. Lau, S., N. Stanhope, …, D. A. Middleton. 2019. Drug orientations within statin-loaded lipoprotein nanoparticles by ^{19}F solid-state NMR. *Chem. Commun.* 55:13287–13290.

24. Mapley, B., D. Townsend, D. A. Middleton…, 2021. ^{19}F solid-state NMR and vibrational Raman characterization of corticosteroid drug-lipid membrane interactions. *ChemPlusChem.* 86:1517–1523.

25. Smith, S. O., J. Hamilton, …, B. J. Bormann. 1994. Rotational resonance NMR determination of intra-and intermolecular distance constraints in dipalmitoylphosphatidylcholine bilayers. *Biochemistry.* 33:6327–6333.

26. Tang, M., A. J. Waring, and M. Hong. 2007. Trehalose-protected lipid membranes for determining membrane protein structure and insertion. *J. Magn. Reson.* 184:222–227.

27. Lin, P., X. Chen, …, D. H. Zhou. 2014. Membrane attachment and structure models of lipid storage droplet protein 1. *Biochim. Biophys. Acta.* 1838:874–881.

28. Hirsh, D. J., J. Hammer, …, J. Schaefer. 1996. Secondary structure and location of a magainin analogue in synthetic phospholipid bilayers. *Biochemistry.* 35:12733–12741.

29. Smith, S. O., T. Kawakami, …, S. Aimoto. 2001. Helical structure of phospholamban in membrane bilayers. *J. Mol. Biol.* 313:1139–1148.

30. Toke, O., W. L. Maloy, …, J. Schaefer. 2004. Secondary structure and lipid contact of a peptide antibiotic in phospholipid bilayers by REDOR. *Biophys. J.* 87:662–674.

31. Toraya, S., K. Nishimura, and A. Naito. 2004. Dynamic structure of vesicle-bound melittin in a variety of lipid chain lengths by solid-state NMR. *Biophys. J.* 87:3323–3335.

32. Shu, N. S., M. S. Chung, …, W. Qiang. 2015. Residue-specific structures and membrane locations of pH-low insertion peptide by solid-state nuclear magnetic resonance. *Nat. Commun.* 6:7787.

33. Griffiths, J. M., A. E. Bennett, R. G. Griffin…, 2000. Structural investigation of the active site in bacteriorhodopsin: geometric constraints on the roles of Asp-85 and Asp-212 in the proton-pumping mechanism from solid-state NMR. *Biochemistry.* 39:362–371.

34. Crocker, E., A. B. Patel, …, S. O. Smith. 2004. Dipolar assisted rotational resonance NMR of tryptophan and tyrosine in rhodopsin. *J. Biomol. NMR.* 29:11–20.

35. Hiller, M., L. Krabben, …, H. Oschkinat. 2005. Solid-state magic-angle spinning NMR of outer-membrane protein G from *Escherichia coli*. *Chembiochem.* 6:1679–1684.

36. Volke, F., and A. Pampel. 1995. Membrane hydration and structure on a subnanometer scale as seen by high resolution solid state nuclear magnetic resonance: POPC and POPC/$C_{12}EO_4$ model membranes. *Biophys. J.* 68:1960–1965.

37. Chen, Z.-J., and R. E. Stark. 1996. Evaluating spin diffusion in MAS-NOESY spectra of phospholipid multibilayers. *Solid State Nucl. Magn. Reson.* 7:239–246.

38. Huster, D., and K. Gawrisch. 1999. NOESY NMR crosspeaks between lipid headgroups and hydrocarbon chains: spin diffusion or molecular disorder? *J. Am. Chem. Soc.* 121:1992–1993.

39. Ramamoorthy, A., and J. Xu. 2013. 2D ^{1}H/^{1}H RFDR and NOESY NMR experiments on a membrane-bound antimicrobial peptide under magic angle spinning. *J. Phys. Chem. B.* 117:6693–6700.

40. Roos, M., T. Wang, …, M. Hong. 2018. Fast magic-angle-spinning ^{19}F spin exchange NMR for determining nanometer ^{19}F–^{19}F distances in proteins and pharmaceutical compounds. *J. Phys. Chem. B.* 122:2900–2911.

41. Arnold, A. A., J.-P. Bourgouin, I. Marcotte…, 2018. Whole cell solid-state NMR study of *Chlamydomonas reinhardtii* microalgae. *J. Biomol. NMR.* 70:123–131.

42. Grobner, G., C. Glaubitz, and A. Watts. 1999. Probing membrane surfaces and the location of membrane-embedded peptides by ^{13}C MAS NMR using lanthanide ions. *J. Magn. Reson.* 141:335–339.

43. Buffy, J. J., T. Hong, M. Hong…, 2003. Solid-state NMR investigation of the depth of insertion of protegrin-1 in lipid bilayers using paramagnetic Mn^{2+}. *Biophys. J.* 85:2363–2373.

44. Kalabekova, R., C. M. Quinn, T. Polenova…, 2024. ^{19}F Fast magic-angle spinning NMR spectroscopy on microcrystalline complexes of fluorinated ligands and the carbohydrate recognition domain of galectin-3. *Biochemistry.* 63:2207–2216.

45. Porat-Dahlerbruch, G., J. Struppe, …, T. Polenova. 2022. ^{19}F fast MAS (60–111 kHz) dipolar and scalar based correlation spectroscopy of organic molecules and pharmaceutical formulations. *Solid State Nucl. Magn. Reson.* 122:101831.

Biophysical Journal, Volume *124*

Supplemental information

Simultaneous assessment of membrane bilayer structure and drug insertion by ^{19}F solid-state NMR

Kiran Kumar, Alexandre A. Arnold, Raphaël Gauthier, Marius Mamone, Jean-François Paquin, Dror E. Warschawski, and Isabelle Marcotte

Supplementary information for:

Simultaneous assessment of membrane bilayer structure and drug insertion by ^{19}F solid-state NMR

Kiran Kumar[1], Alexandre A. Arnold[1], Raphaël Gauthier[2], Marius Mamone[2], Jean-François Paquin[2], Dror E. Warschawski[1,3*] & Isabelle Marcotte[1*]

[1]Departement of Chemistry, Université du Québec à Montréal, P.O. Box 8888, Downtown Station, Montreal, Canada H3C 3P8

[2]PROTEO, CCVC, Département de chimie, Université Laval, 1045 Avenue de la Médecine, Québec, Québec, G1V 0A6, Canada

[3]Laboratoire des Biomolécules, LBM, CNRS UMR 7203, Sorbonne Université, École normale supérieure, PSL University, 75005 Paris, France

*Corresponding authors

Isabelle Marcotte
Tel: 1-514-987-3000 #5015
Fax: 1-514-987-4054
E-mail : *marcotte.isabelle@uqam.ca*

Dror E. Warschawski
Tel : +33 1 44 27 32 16
Fax : +33 1 44 27 62 50
E-mail : *Dror.Warschawski@Sorbonne-Universite.fr*

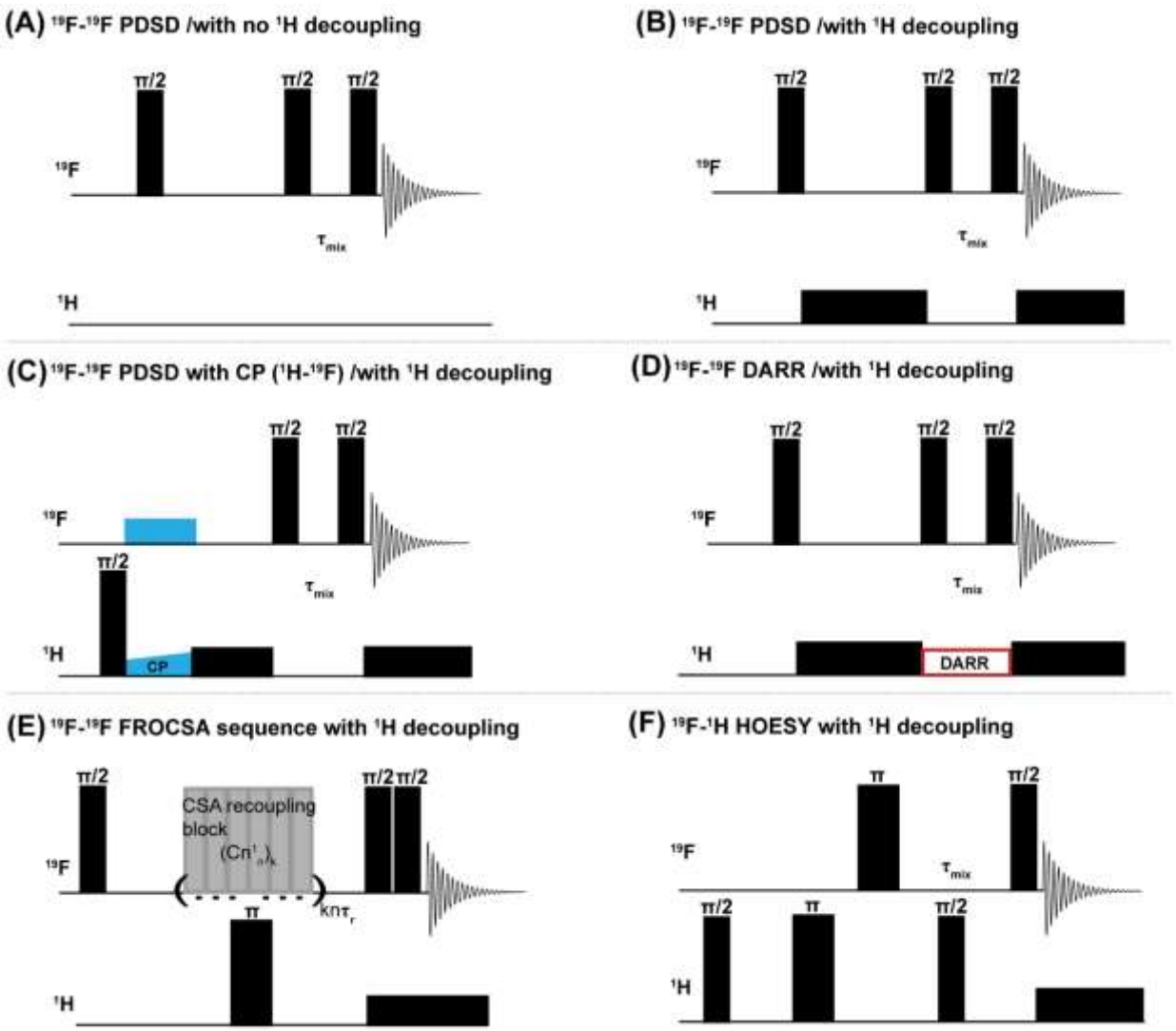

Figure S1: Typical pulse sequences schemes used in this article: (A, B & C) 2D ^{19}F-^{19}F PDSD, (D) ^{19}F-^{19}F DARR, (E) ^{19}F-^{19}F FROCSA and (F) ^{19}F-^{1}H HOESY experiments.

Additional spectra and assignments of rosuvastatin :

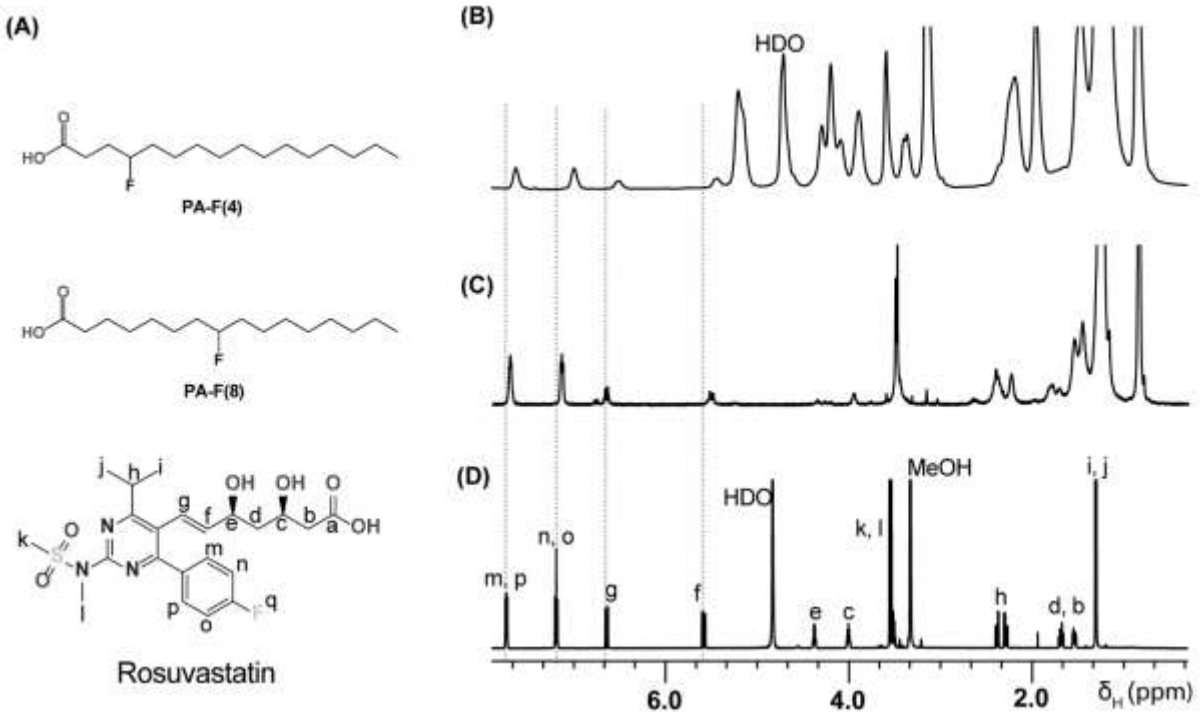

Figure S2: (A) Fluorinated palmitic acids (PAs) used in this work, and ^{1}H annotation in rosuvastatin (RVS). (B) ^{1}H SS-NMR spectrum of POPC/PA-F(4)/PA-F(8) at a molar ratio of 4:1:1, with RVS at a lipid/PAs/RVS molar ratio of 40:20:3 in D_2O, using a MAS frequency of 10 kHz MAS. ^{1}H solution NMR spectrum of (C) DPC-d_{31}/PA-F(4)/PA-F(8) at a molar ratio of 2:1:1, with RVS at a DPC-d_{31}/PAs/RVS molar ratio of 20:20:10 in D_2O, and of (D) RVS in MeOH. Experiments (C) and (D) were recorded using a Bruker Avance spectrometer operating at 600 MHz (Milton, ON, Canada) equipped with a 5 mm solution NMR probe. All experiments were performed at 30 °C.

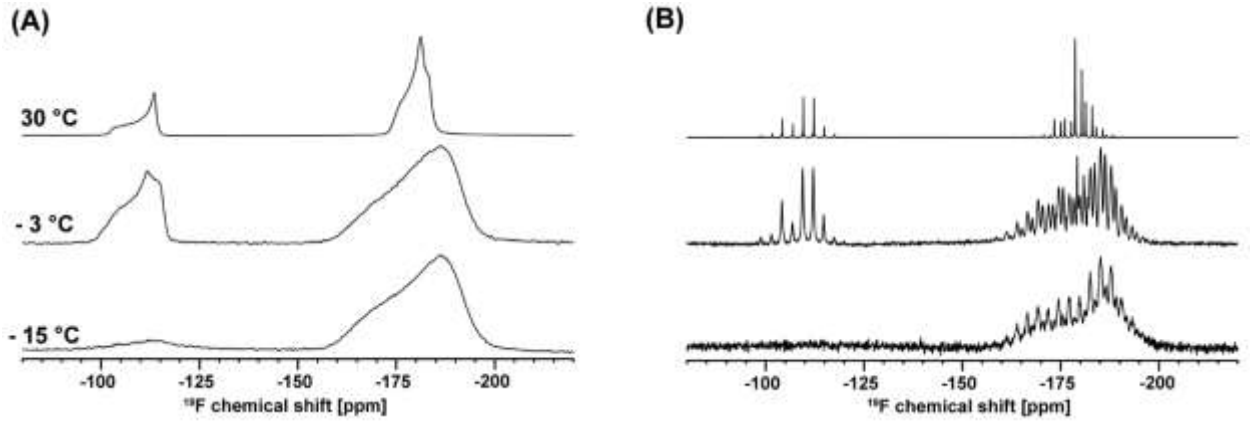

Figure S3: (A) Static and (B) 1 kHz MAS ^{19}F SS-NMR spectra of POPC model membranes incorporating monofluorinated PAs, at a POPC/PA-F(4)/PA-F(8) molar ratio of 4:1:1, with RVS at a lipid/PAs/RVS molar ratio of 40:20:3. Experiments were performed at different temperatures with ^{1}H decoupling. PA resonances are on the right (*circa* -180 ppm), while statin resonances are on the left (*circa* -105 ppm).

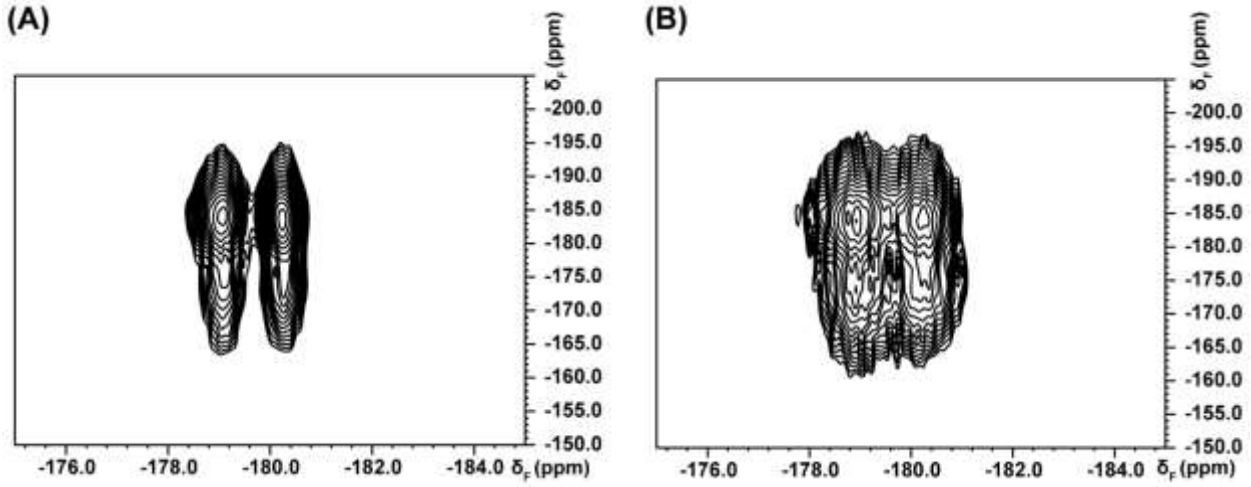

Figure S4: 2D ^{19}F-^{19}F FROCSA spectrum of POPC model membranes incorporating monofluorinated PAs, at a POPC/PA-F(4)/PA-F(8) molar ratio of 4:1:1. (A) at -3 $^{\circ}$C and (B) at -15 $^{\circ}$C. Experiments were performed at 11 kHz MAS with ^{1}H decoupling.

Additional information regarding sparfloxacin:

Sparfloxacin (SPX) is a fluoroquinolone with two fluorine atoms separated by a distance of 4.73 Å (**Fig. S5A**), and presents two polymorphs in the pure compound. Previous theoretical studies have shown that similar types of molecules interact with lipid membranes, fluoroquinolones being found either on the surface or in the core of the bilayer, depending on the pH [1]. When SPX is incorporated into dipalmitoylphosphatidylcholine (DPPC) model membranes at a molar ratio of 1:2, the two polymorphs are reduced to a single component. As seen in **Fig. S5B**, the two fluorine nuclei of SPX have isotropic chemical shifts of -85.1 ppm and -76.8 ppm, and noticeable differences in CSA values of -85.1 ppm (32 kHz) and -76.8 ppm (29 kHz), respectively.

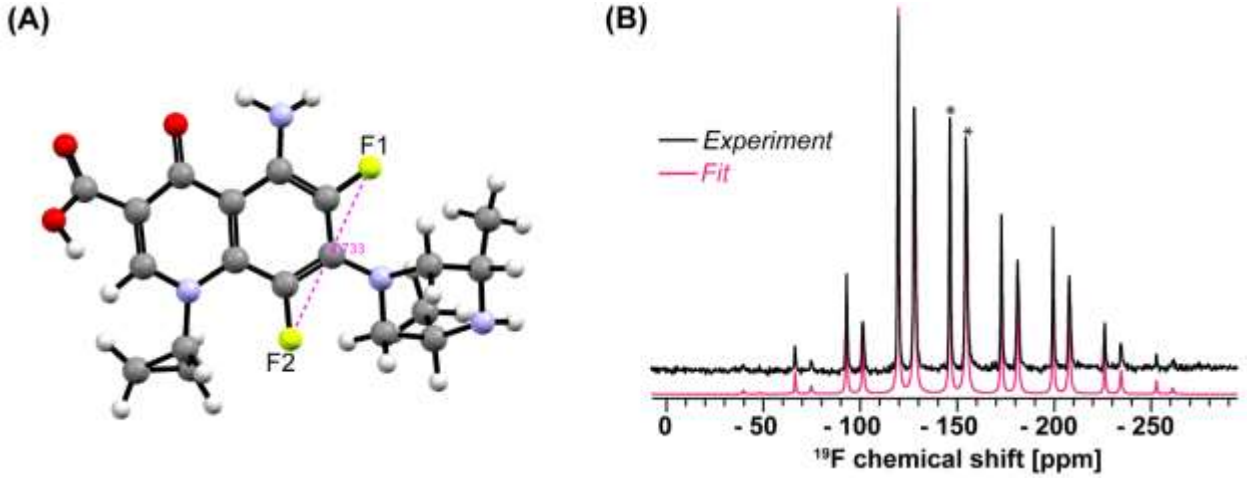

Figure S5: (A) DFT-optimized structure of sparfloxacin (SPX) and (B) ^{1}H-^{19}F CP MAS SS-NMR spectrum of the drug in DPPC membranes at a DPPC/SPX molar ratio of 2:1. Experiments were performed at 5 $^{\circ}$C with ^{1}H decoupling, and MAS at 10 kHz. Asterisks (*) refer isotropic peaks.

Direct intramolecular ^{19}F-^{19}F dipolar coupling measurement by 2D RFDR in SPX incorporated into DPPC model membranes is possible and, with a value of 5 Å, is in good agreement with the DFT-derived distance (**Fig. S5 & Fig. S6**). 2D ^{19}F-^{19}F PDSD and DARR spectra can also be obtained (**Fig. S6**). The peaks are well resolved, even at a moderate MAS frequency of 10 kHz, and correlation cross peaks are clearly noticeable.

[1] O. Cramariuc, T. Rog, M. Javanainen, L. Monticelli, A.V. Polishchuk, I. Vattulainen, Mechanism for translocation of fluoroquinolones across lipid membranes, Biochim. Biophys. Acta-Biomembr. 1818 (2012) 2563-2571.

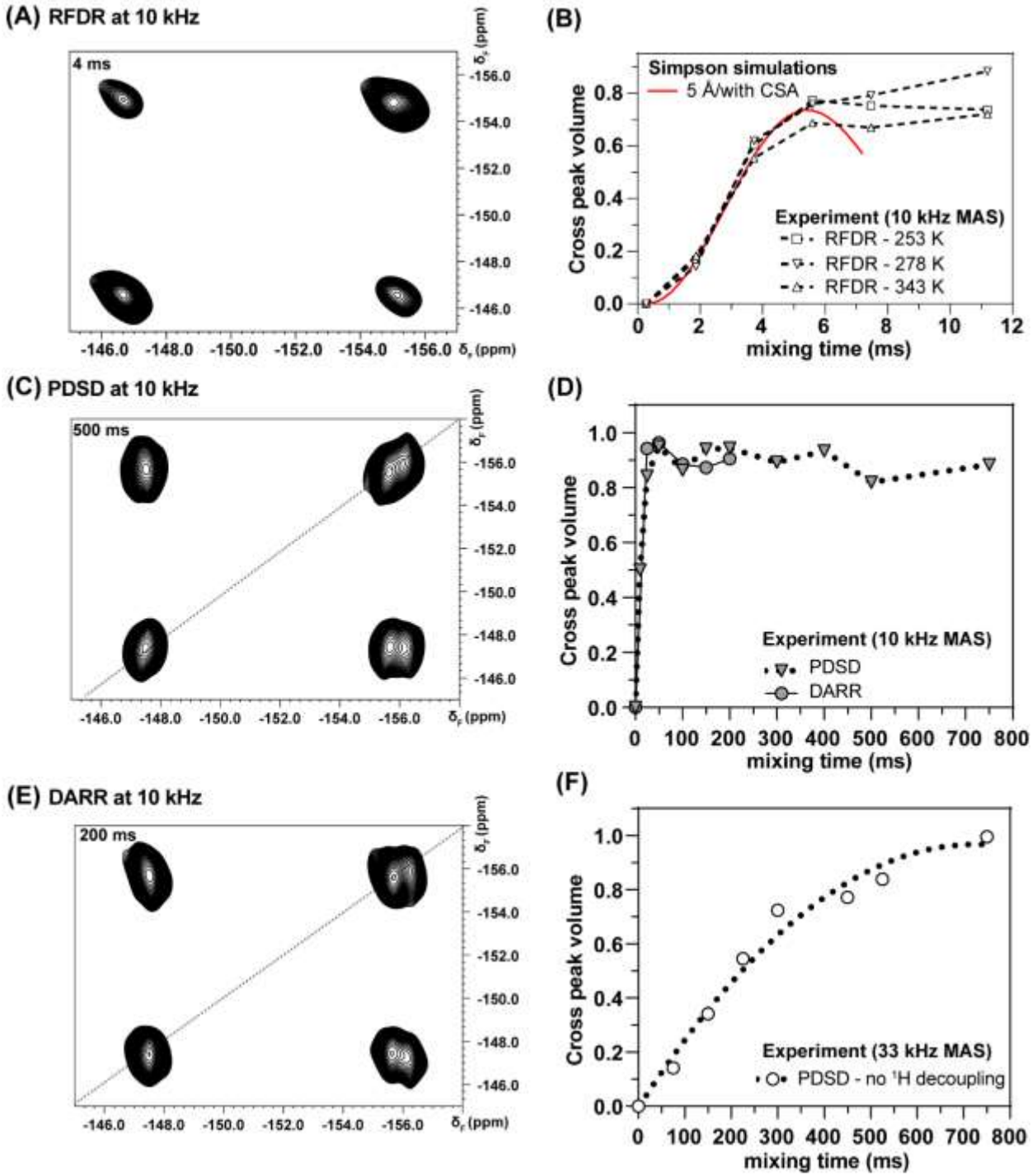

Figure S6: 2D ^{19}F-^{19}F SS-NMR correlation spectra of sparfloxacin (SPX) in DPPC sample (DPPC/SPX molar ratio of 2:1). (A) 2D ^{19}F-^{19}F RFDR spectrum at 4 ms mixing time, obtained at 5 $^{\circ}$C, and 10 kHz MAS with ^{1}H decoupling. (B) RFDR buildup curves obtained at various temperatures, together with a simulation curve obtained with the Simpson software. (C) 2D ^{19}F-^{19}F PDSD spectrum at 500 ms mixing time, obtained at 5 $^{\circ}$C, and 10 kHz MAS with ^{1}H decoupling. (D) PDSD and DARR buildup curves obtained at 5 $^{\circ}$C, and 10 kHz MAS with ^{1}H decoupling. (E) 2D ^{19}F-^{19}F DARR spectrum at 200 ms mixing time, obtained at 5 $^{\circ}$C, and 10 kHz MAS with ^{1}H decoupling. (F) PDSD buildup curve obtained at 5 $^{\circ}$C, and 33 kHz MAS, without ^{1}H decoupling.

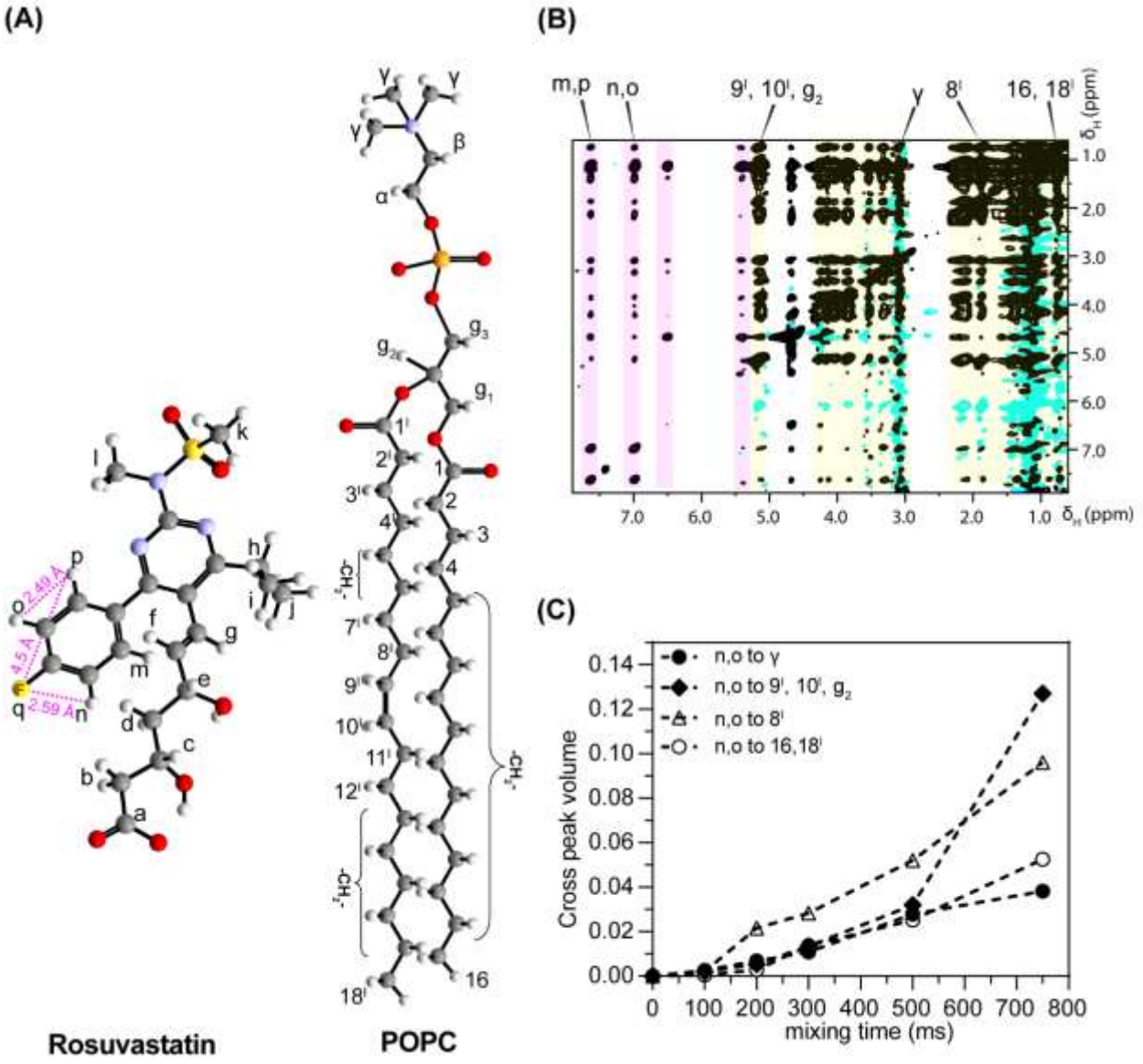

Figure S7: Attempt at locating rosuvastatin in model membranes. (A) DFT-optimized structure of RVS with ^{1}H annotation for RVS and POPC. (B) 10 kHz MAS ^{1}H-^{1}H 2D NOESY spectrum with a 500 ms mixing time, of RVS incorporated into POPC/PA-F(4)/PA-F(8) (molar ratio 4:1:1), with a lipid/PAs/RVS molar ratio of 40:20:3. (C) NOESY buildup curve for the cross peaks between the aromatic statin protons and the lipid protons. Experiments were performed at 35 ˚C. Black peaks are positive cross peaks. Blue peaks are negative signals that can be considered as artifacts.